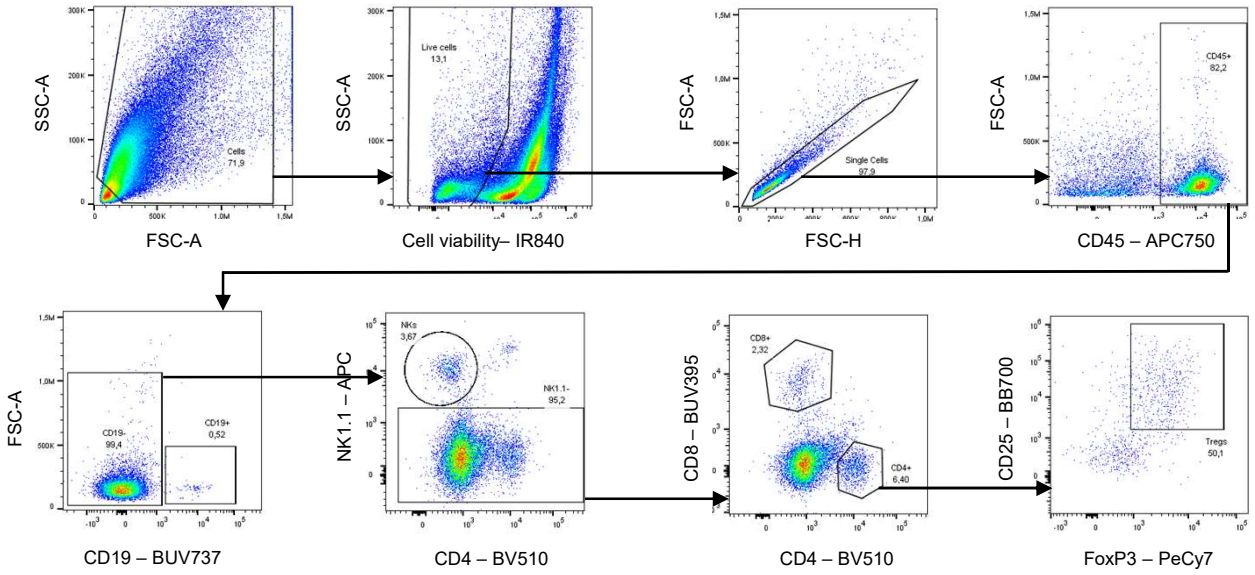

Supplementary Figure 1. Flow cytometry gating strategy for the analysis of lymphocytes. Debris and dead cells were excluded using forward/side scatter (FSC-A/SSC-A) and PromoFluor 840. FSC-H and FSC-A excluded doublets. B cells ($CD19^+$) were gated from the leucocyte ($CD45^+$ cells) gate, and NK cells ($NK1.1^+$) from the $CD19^-$ gate. CD8 T cells ($CD8^+$), CD4 T cells ($CD4^+$) and Treg cells ($CD4^+$ $CD25^+$ $FoxP3^+$) were selected from the $CD19^-$ $NK1.1^-$ gate.

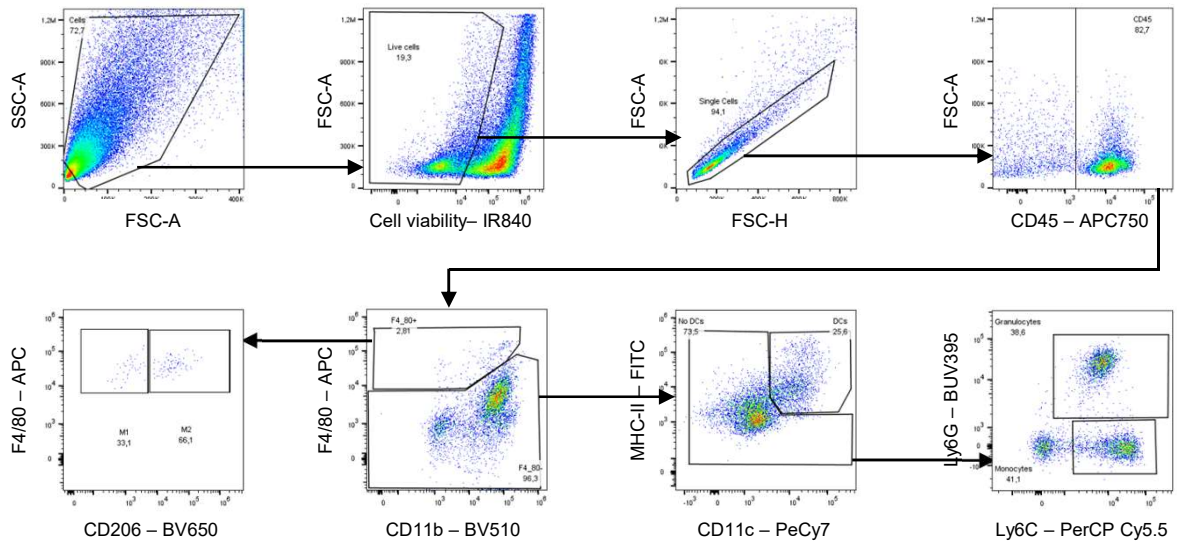

Supplementary Figure 2. Flow cytometry gating strategy for the analysis of myeloid cell populations. Debris and dead cells were excluded using forward/side scatter (FSC-A/SSC-A) and PromoFluor 840. FSC-H and FSC-A was used to exclude doublets. Leucocytes ($CD45^+$ cells) were first classified into macrophages ($CD11b^+$ $F4/80^+$). From the negative gate of these cells, DCs were gated as $CD11c^+$ $MHC\text{-}II^+$. Granulocytes ($CD11b^+$ $Ly6G^{high}$ $Ly6C^{low}$) and monocytes ($CD11b^+$ $Ly6G^-$ $Ly6C^{high}$) were selected from the exclusion gate of DCs. Within the macrophage population, $CD206^-$ cells were classified as M1-like macrophages, and $CD206^+$ cells as M2-like macrophages.

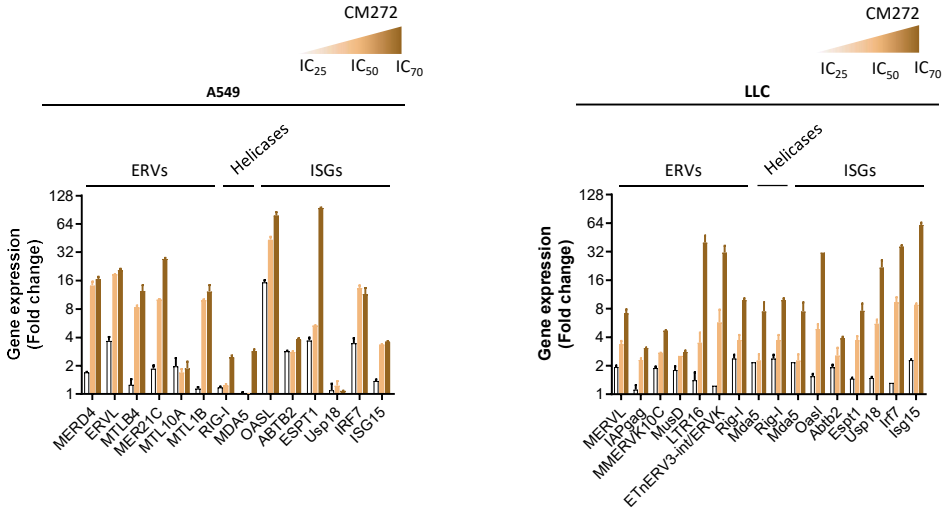

Supplementary Figure 3. Mean relative expression of ERVs, helicases and ISGs, measured by real-time PCR, in human (A549) and mouse (LLC) lung cancer cell lines.

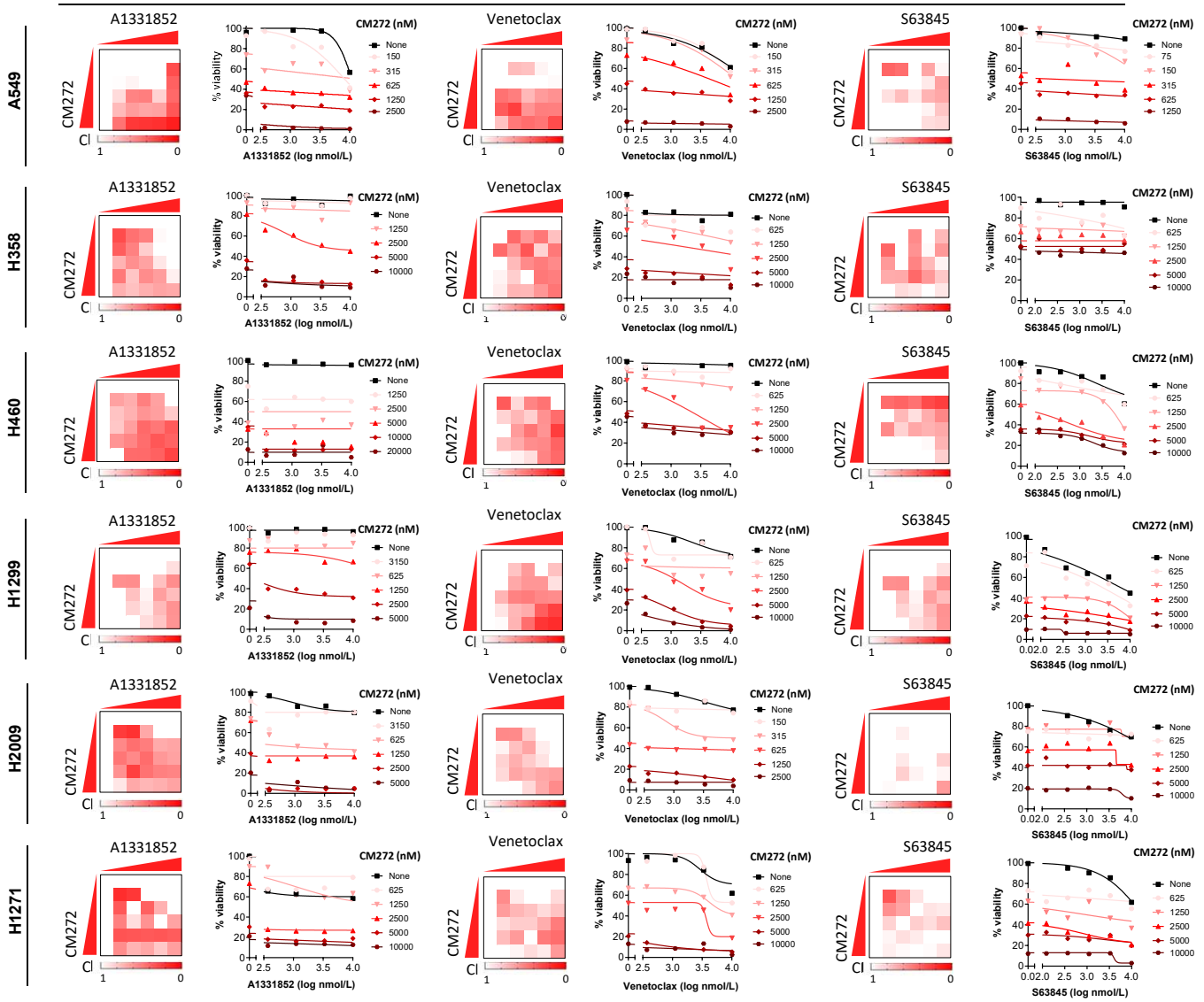

Supplementary Figure 4. Combination index (CI) values and cell viability curves obtained after incubation of the indicated human lung cancer cell lines with CM272 and A1331852 (anti-BCL-XL; left), venetoclax (anti-BCL2; middle) or S63845 (anti-MCL1; right) at increasing concentrations. A synergistic effect between the two drugs was considered when at least four drug-drug interactions had CI values < 1.

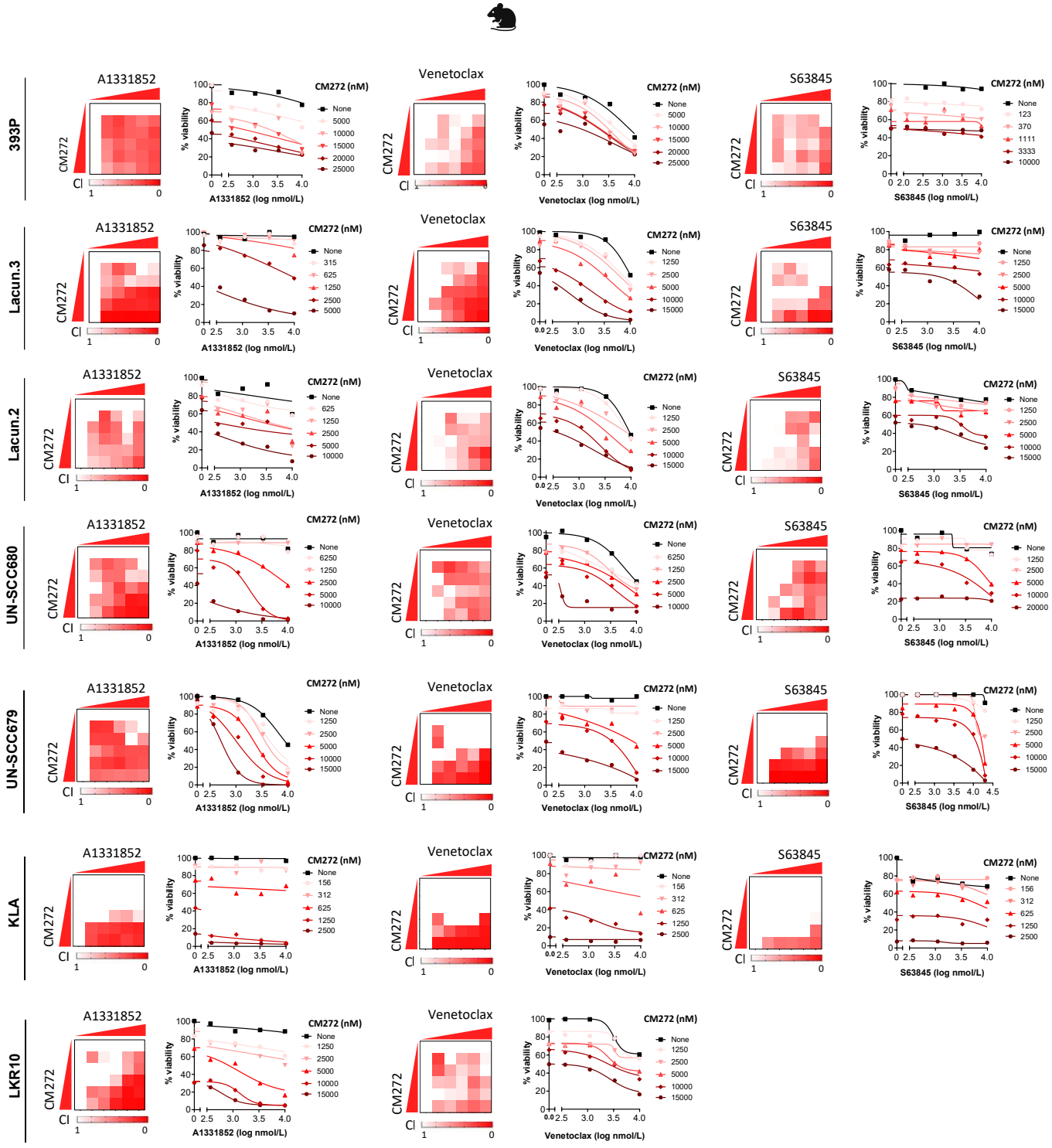

Supplementary Figure 5. Combination index (CI) values and cell viability curves obtained after incubation of the indicated mouse lung cancer cell lines with CM272 and A1331852 (anti-BCL-XL; left), venetoclax (anti-BCL2; middle) or S63845 (anti-MCL1; right) at increasing concentrations. A synergistic effect between the two drugs was considered when at least four drug-drug interactions had CI values < 1.

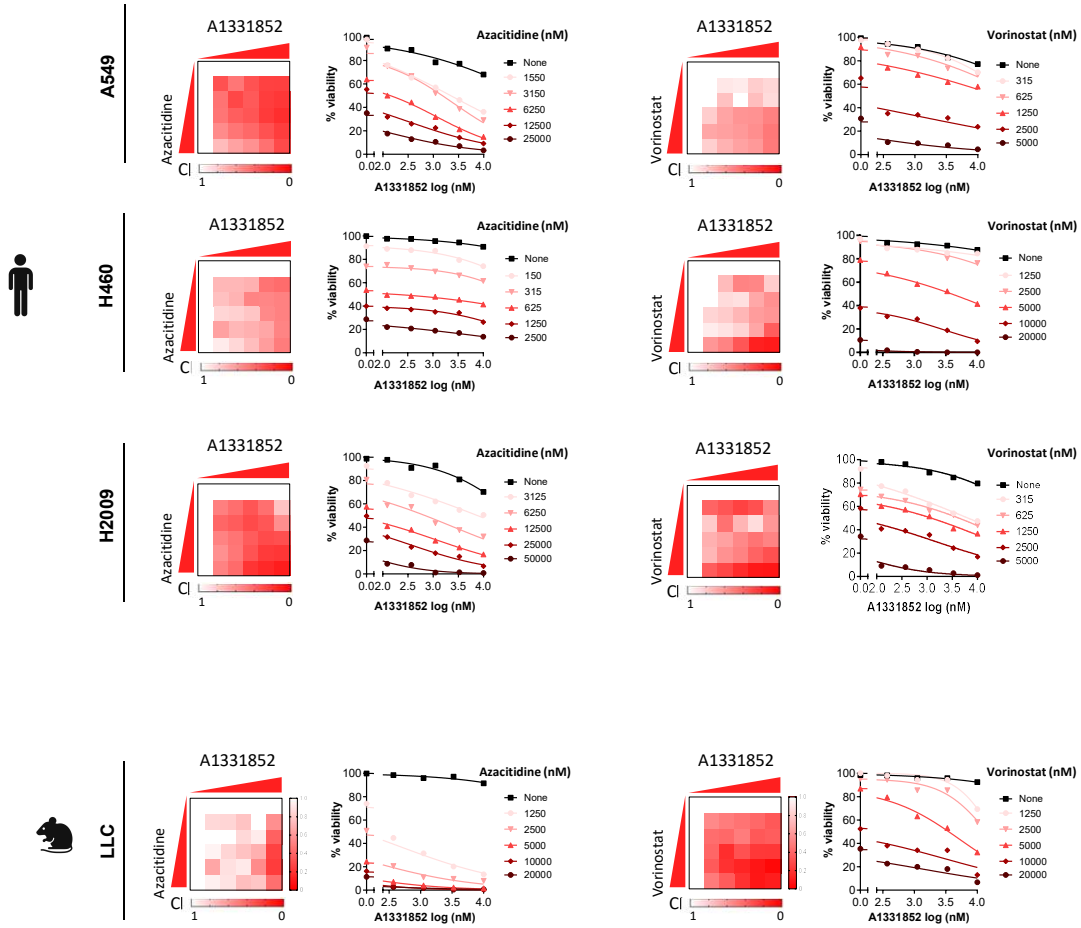

Supplementary Figure 6. Combination index (CI) values and cell viability curves obtained after the treatment of human and mouse lung cancer cells with the epigenetic drugs azacitidine (left) or vorinostat (right) in combination with the anti-BCL-XL A1331852 at increasing concentrations. A synergistic effect between the two drugs was considered when at least four drug-drug interactions had CI values < 1.

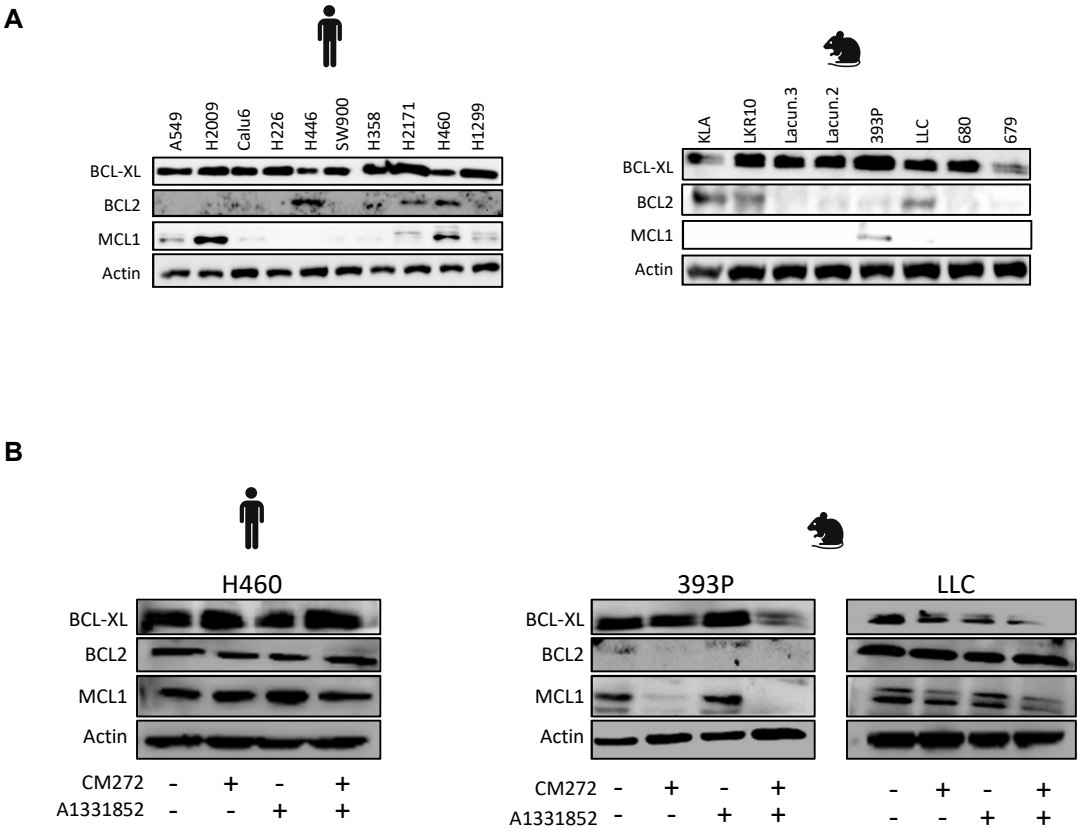

Supplementary Figure 7. **A.** Western blot analysis of the expression of antiapoptotic proteins BCL-XL, BCL2 and MCL1 in human (left) and mouse (right) lung cancer cell lines. **B.** Western blot analysis of the expression of antiapoptotic proteins BCL-XL, BCL2 and MCL1 in human (left) and mouse (right) lung cancer cell lines after the indicated treatments.

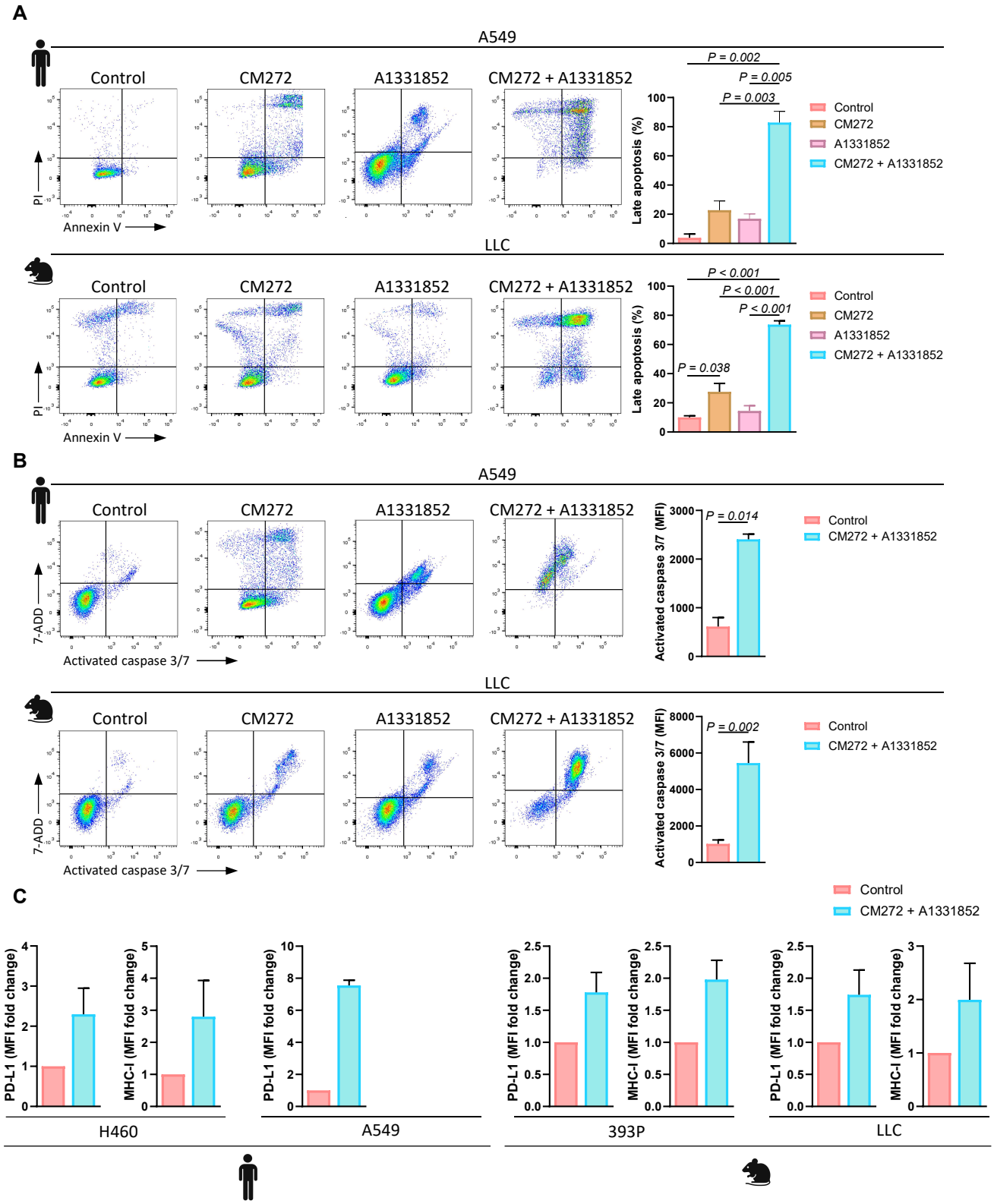

Supplementary Figure 8. **A.** Left panel: Representative Annexin V/PI staining of human (A549) and mouse (LLC) lung cancer cells following treatment with the epigenetic drug CM272 and the BCL-XL inhibitor A1331852. Right panel: Quantification of late apoptotic cells (high Annexin V and PI staining) from three independent experiments. **B.** Representative activated caspase 3/7 and 7-ADD staining of human (A549) and mouse (LLC) lung cancer cells following treatment with the epigenetic drug CM272 and the BCL-XL inhibitor A1331852. Right panel: Quantification of high active caspase 3/7 and 7-ADD staining from three independent experiments performed only with the control and the double treatment groups. **C.** Quantification of PD-L1 and MHC-I staining of human (H460 and A549) and mouse (393) and LLC) lung cancer cells following treatment with the epigenetic drug CM272 and the BCL-XL inhibitor A1331852 from two independent experiments. Treatment conditions were: H460: 5 μM CM272 / 2.5 μM A1331852; A549: 15 μM CM272, 5 μM A1331852; 393P and LLC: 30 μM CM272 / 2.5 μM A1331852. Cells were treated for 24 hours. Data are presented as mean ± SEM. Statistical comparisons between treatment groups were conducted using one-way ANOVA followed by Tukey's post hoc test or Student's t-test.

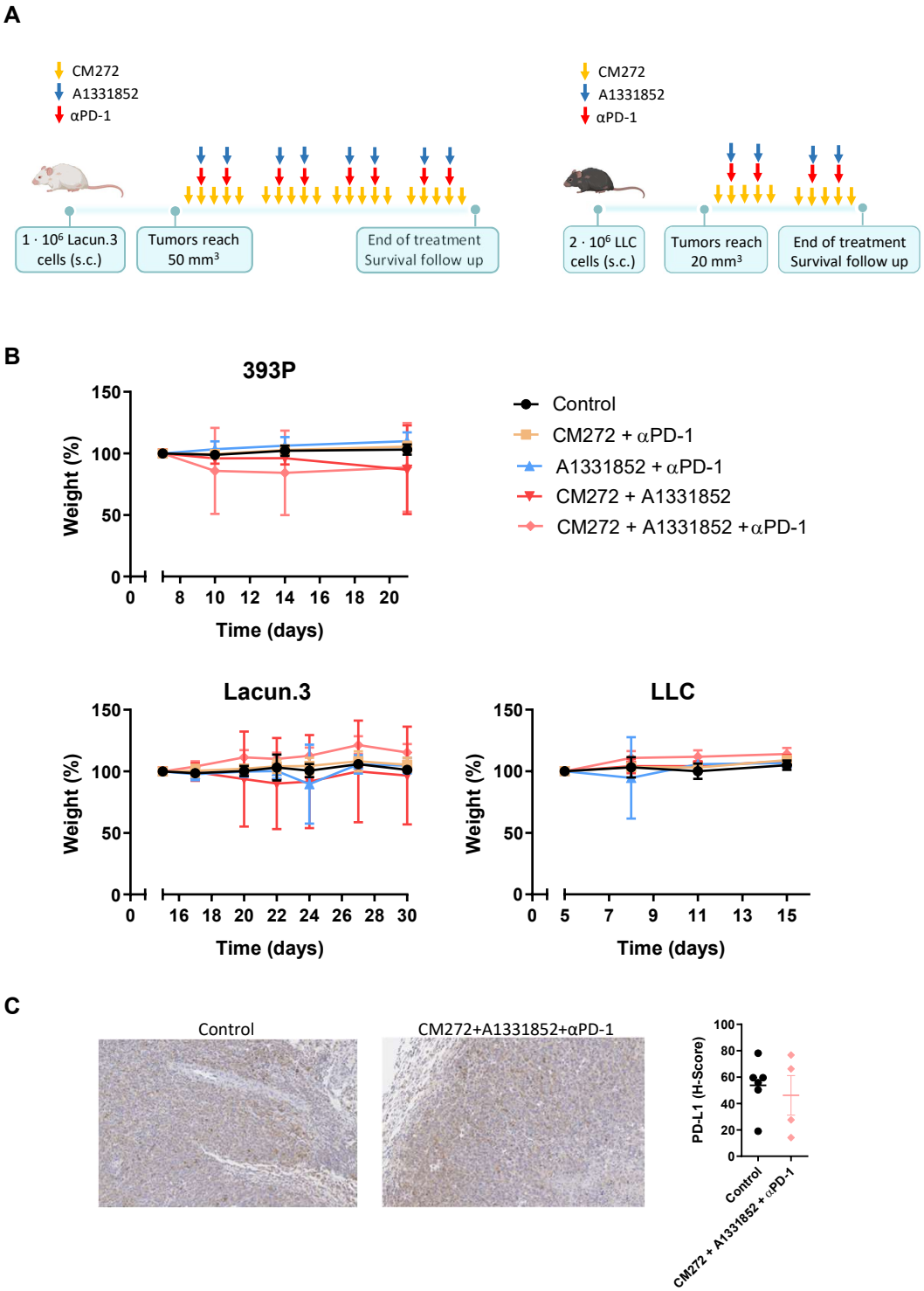

Supplementary Figure 9. **A.** Schematic representation of the therapeutic regimens followed in the *in vivo* cancer models based on subcutaneous inoculation of Lacun.3 (left) or LLC (right) lung cancer cells. **B.** Weight of treated tumor-bearing mice compared to control group. Data from mice bearing 393P, Lacun.3 or LLC tumors are shown. **C.** PD-L1 expression in orthotopic LLC tumors treated with vehicle (control) or the triple combination (CM272/A1331852/anti-PD-1). Left: representative images. Right: Quantification. Data are expressed as mean ± SEM. Comparisons between treatment strategies were performed by Student's t-test.

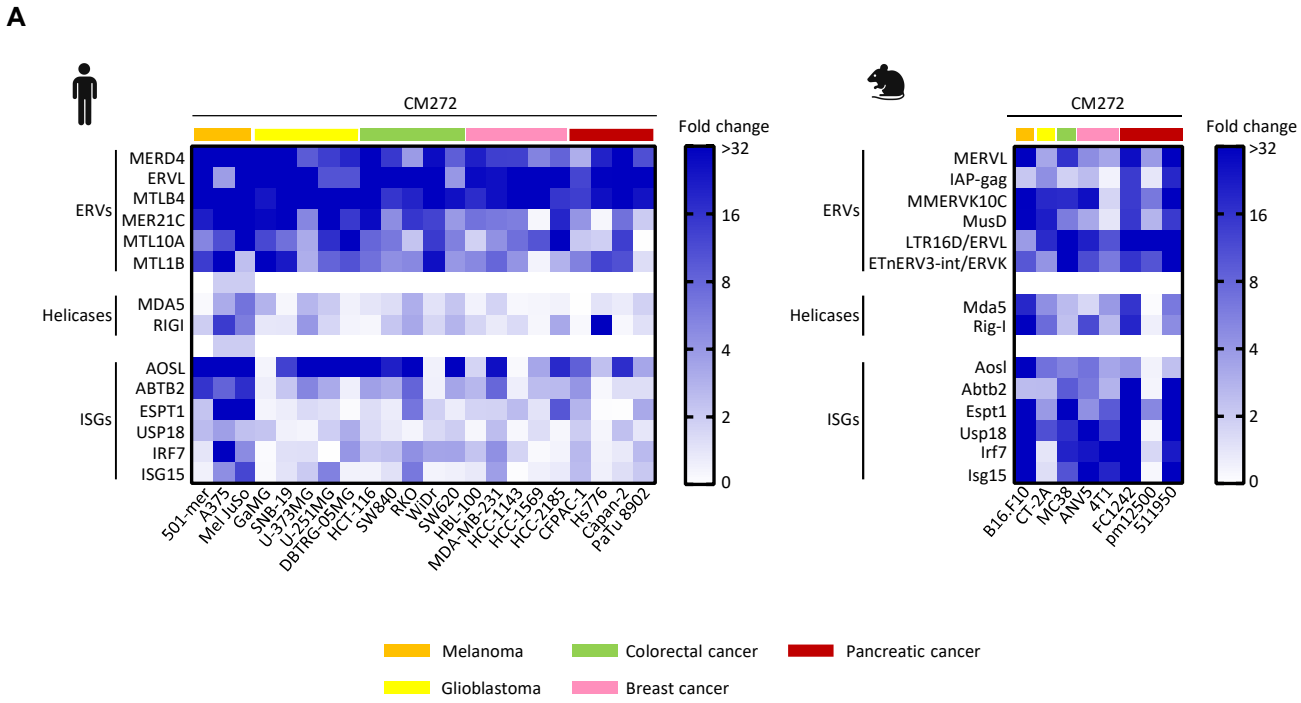

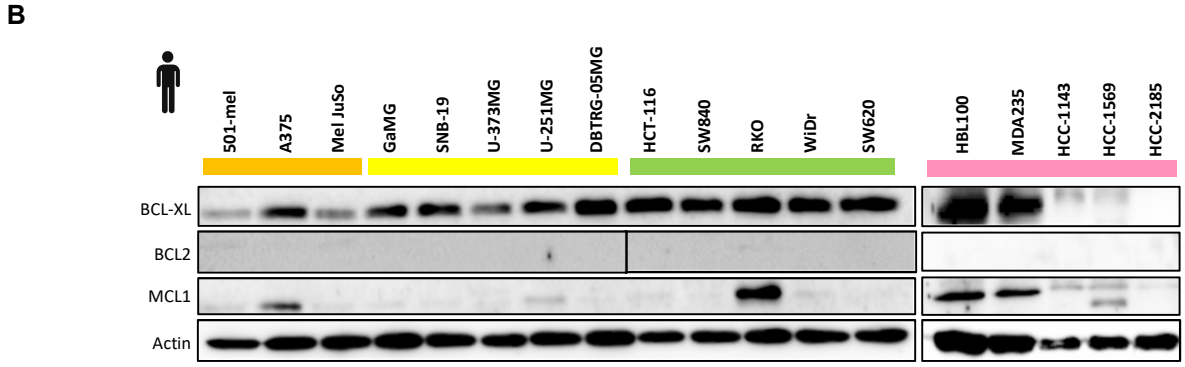

Supplementary Figure 10. **A**. Heatmap of induced mean relative expression of endogenous retroviruses (ERVs), helicases and interferon-stimulated genes (ISGs) after treatment of human (left) and mouse (right) cancer cell lines from melanoma, glioblastoma, colorectal cancer, breast cancer and pancreatic cancer after treatment with CM272. The expression was measured by real-time PCR. **B.** Western blot analysis of the expression of the antiapoptotic proteins BCL-XL, BCL2 and MCL1 in human melanoma, glioblastoma, colorectal cancer and breast cancer cell lines.

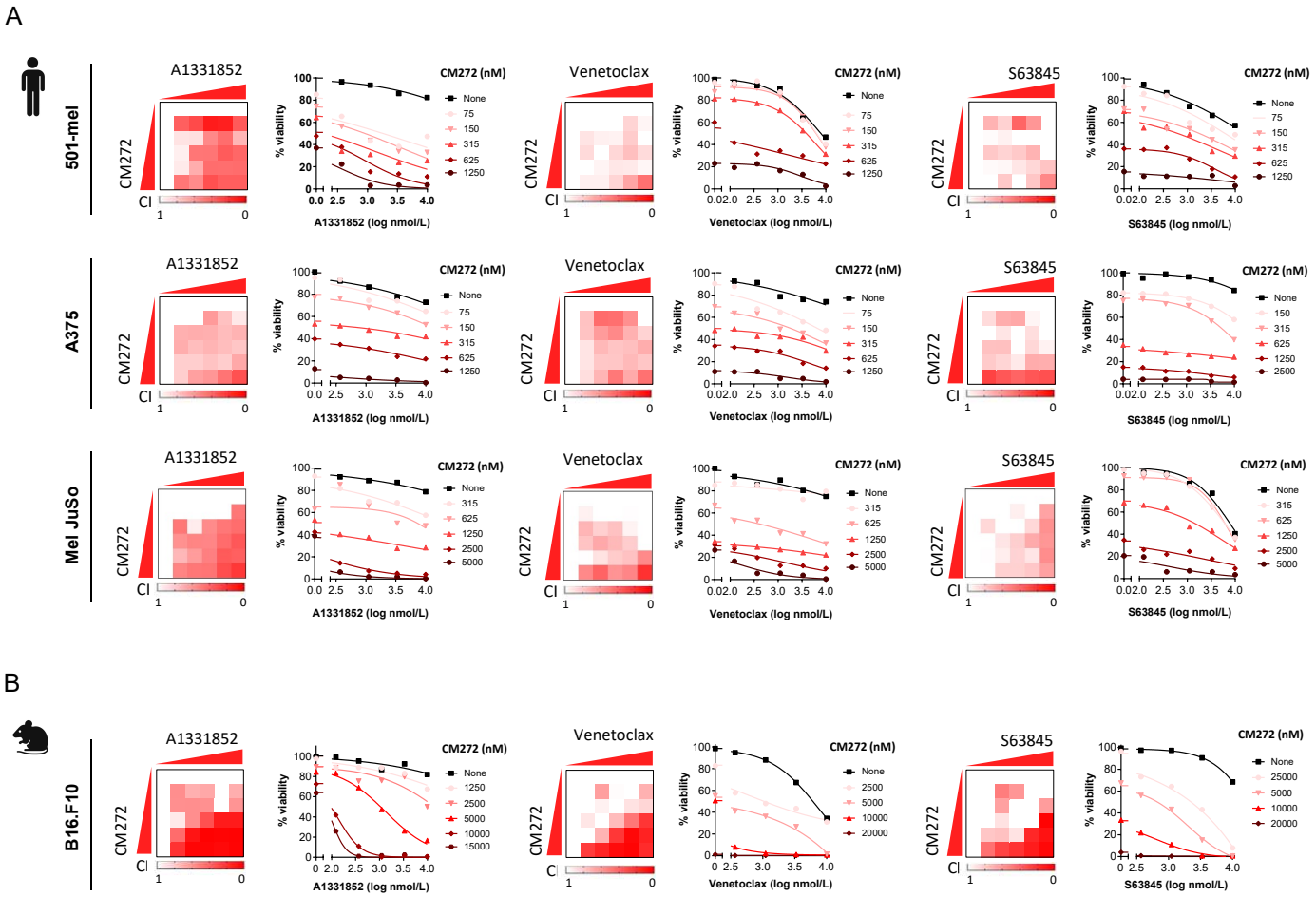

Supplementary Figure 11. Combination index (CI) values and cell viability curves of CM272 with anti-BCL-XL (A1331852, left), anti-BCL2 (venetoclax, middle) or anti-MCL1 (S63845, right) at increasing concentrations in human (**A**) and mouse (**B**) melanoma cell lines. A synergistic effect between the two drugs was considered when at least four drug-drug interactions had CI values < 1.

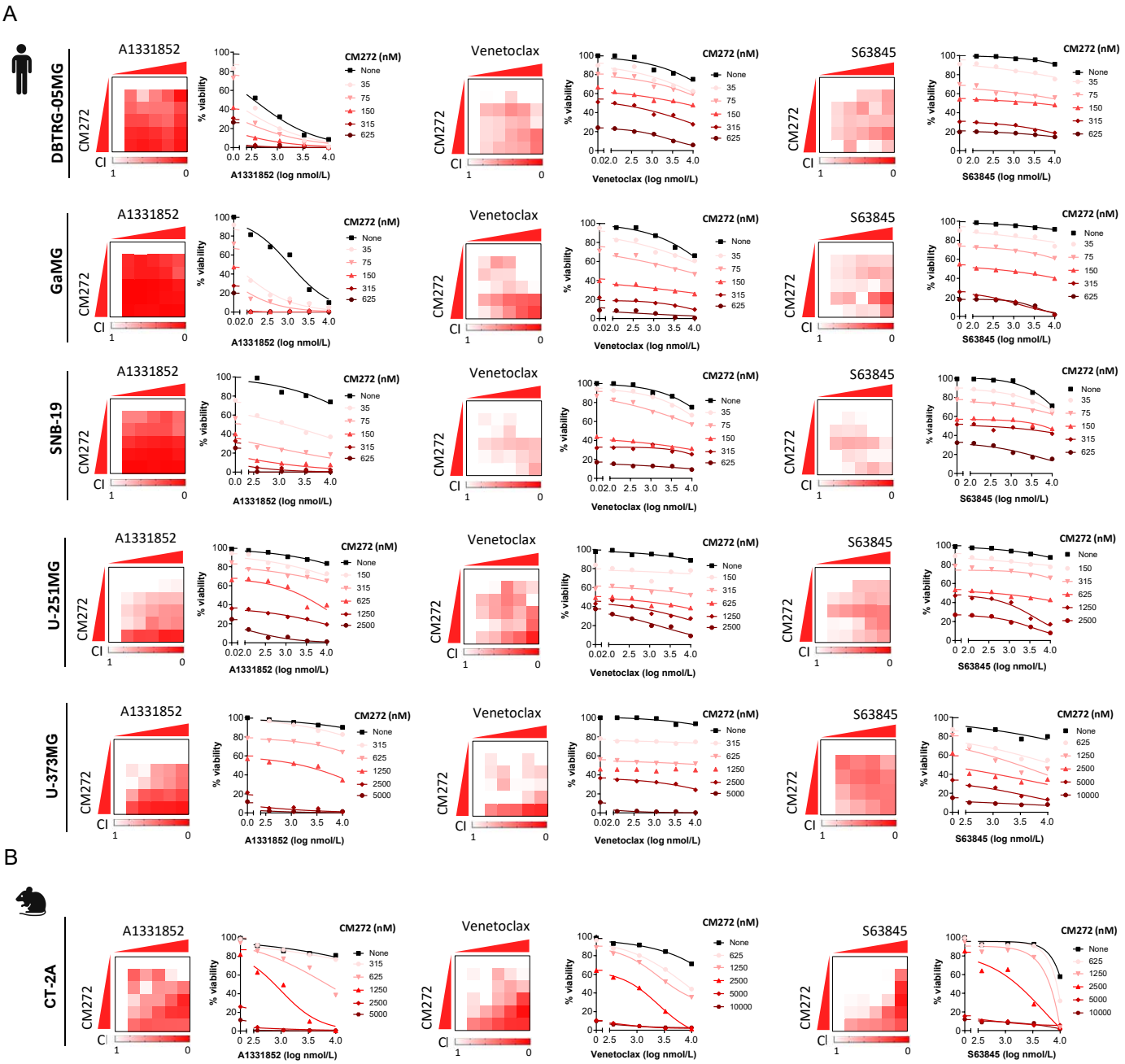

Supplementary Figure 12. Combination index (CI) values and cell viability curves of CM272 with anti-BCL-XL (A1331852, left), anti-BCL2 (venetoclax, middle) or anti-MCL1 (S63845, right) at increasing concentrations in human (**A**) and mouse (**B**) glioblastoma cell lines. A synergistic effect between the two drugs was considered when at least four drug-drug interactions had CI values < 1.

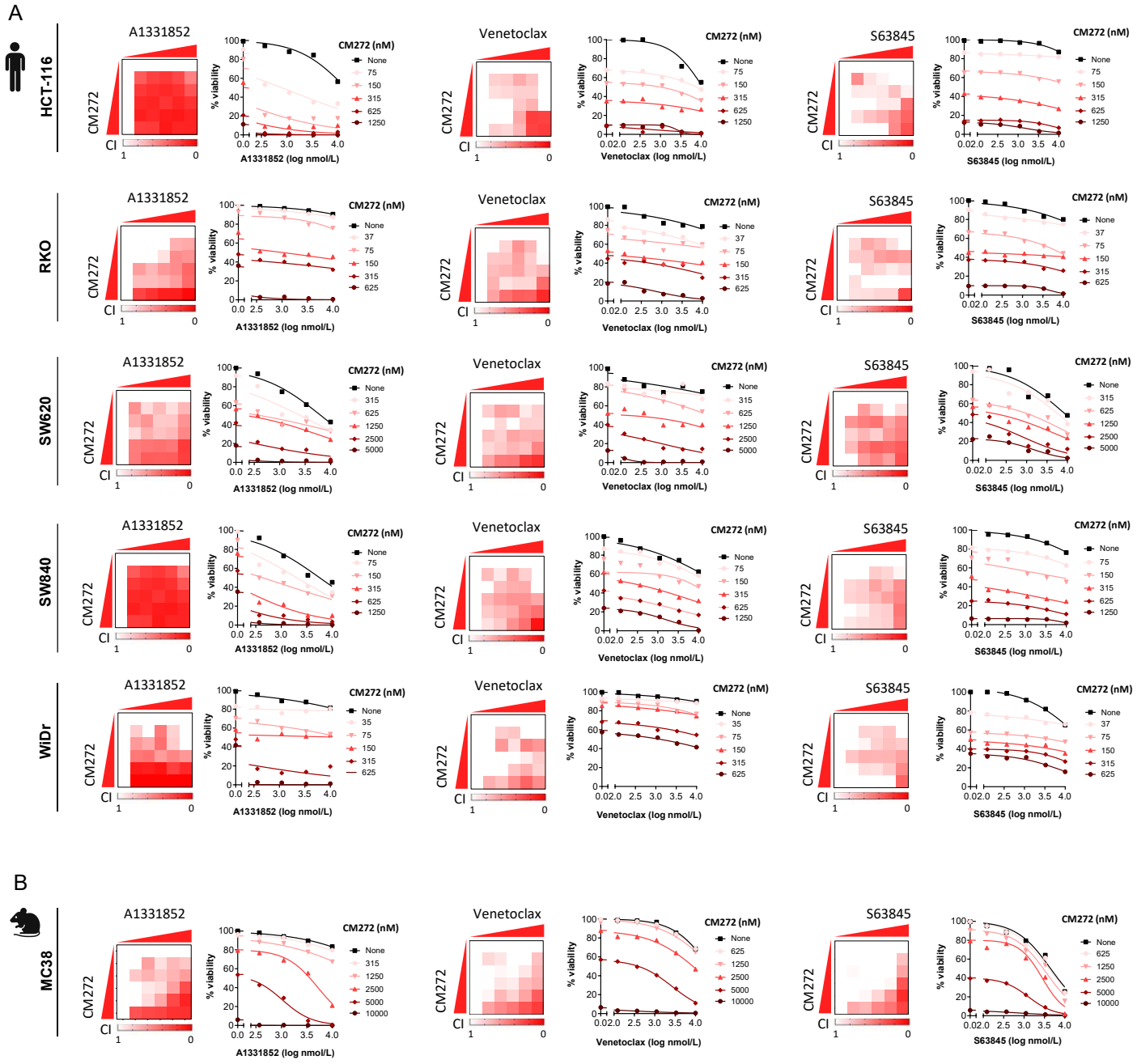

Supplementary Figure 13. Combination index (CI) values and cell viability curves of CM272 with anti-BCL-XL (A1331852, left), anti-BCL2 (venetoclax, middle) or anti-MCL1 (S63845, right) at increasing concentrations in human (**A**) and mouse (**B**) colorectal cancer cell lines. A synergistic effect between the two drugs was considered when at least four drug-drug interactions had CI values < 1.

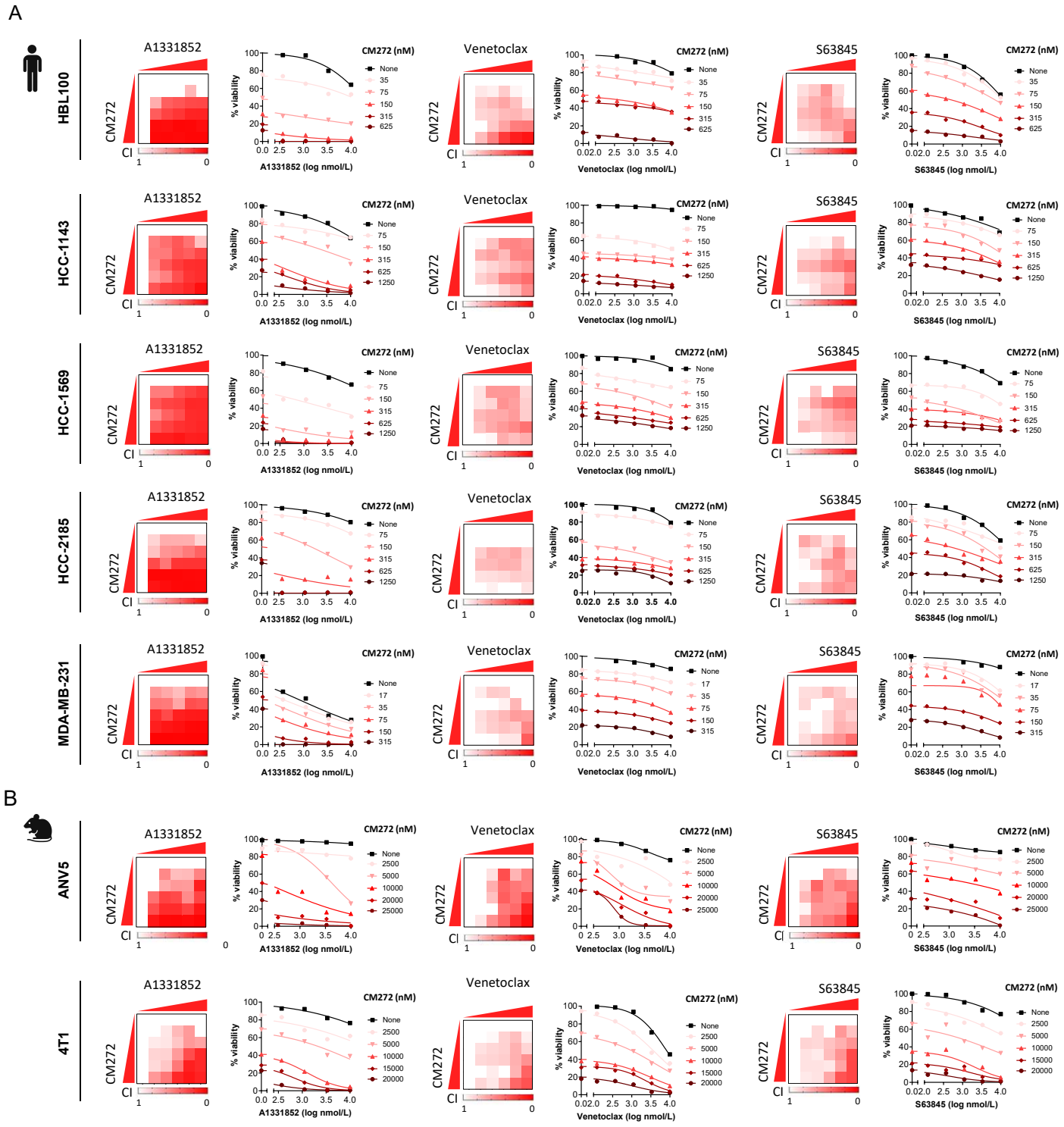

Supplementary Figure 14. Combination index (CI) values and cell viability curves of CM272 with anti-BCL-XL (A1331852, left), anti-BCL2 (venetoclax, middle) or anti-MCL1 (S63845, right) at increasing concentrations in human (**A**) and mouse (**B**) breast cancer cell lines. A synergistic effect between the two drugs was considered when at least four drug-drug interactions had CI values < 1.

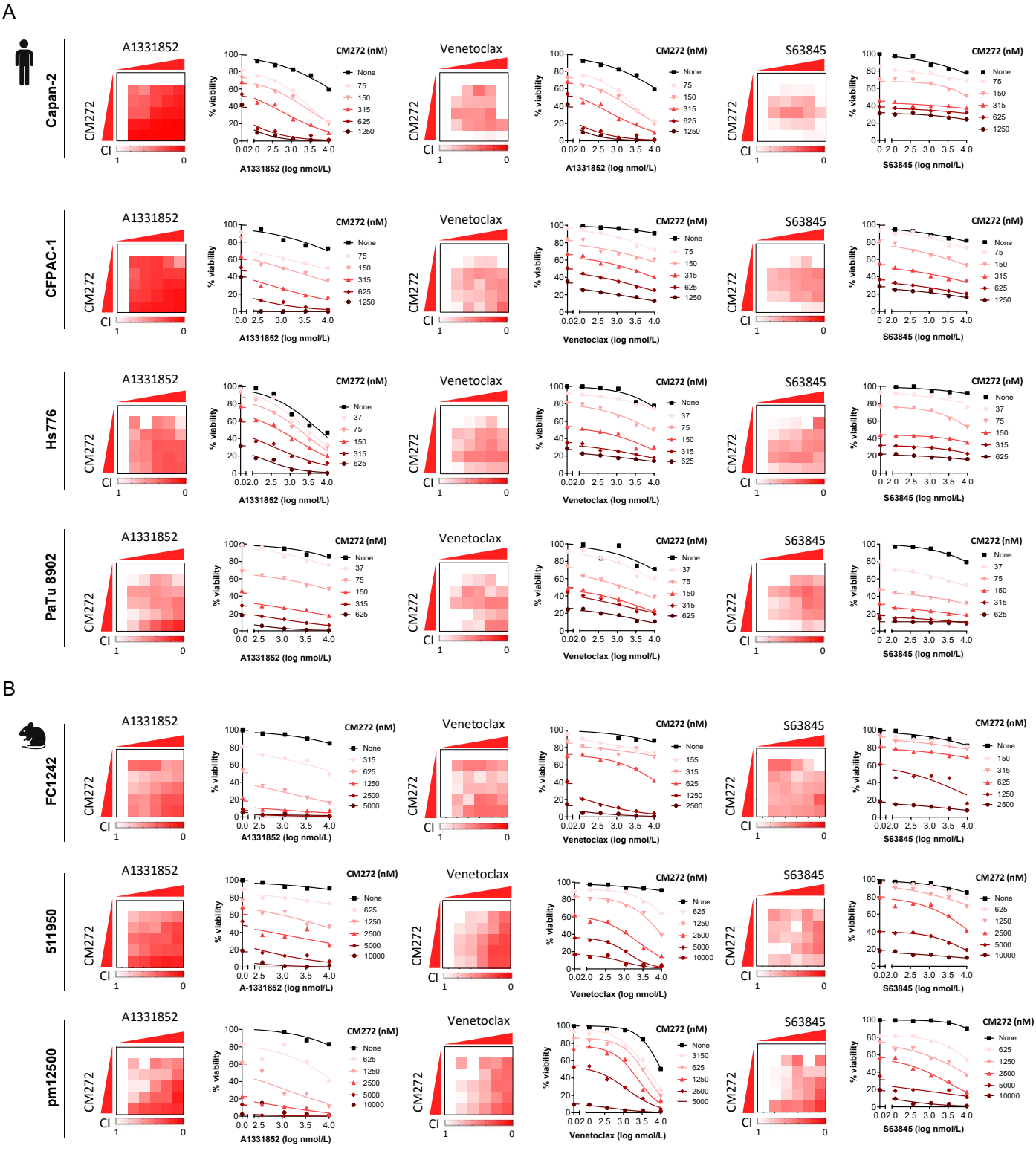

Supplementary Figure 15. Combination index (CI) values and cell viability curves of CM272 with anti-BCL-XL (A1331852, left), anti-BCL2 (venetoclax, middle) or anti-MCL1 (S63845, right) at increasing concentrations in human (**A**) and mouse (**B**) pancreatic cancer cell lines. A synergistic effect between the two drugs was considered when at least four drug-drug interactions had CI values < 1.

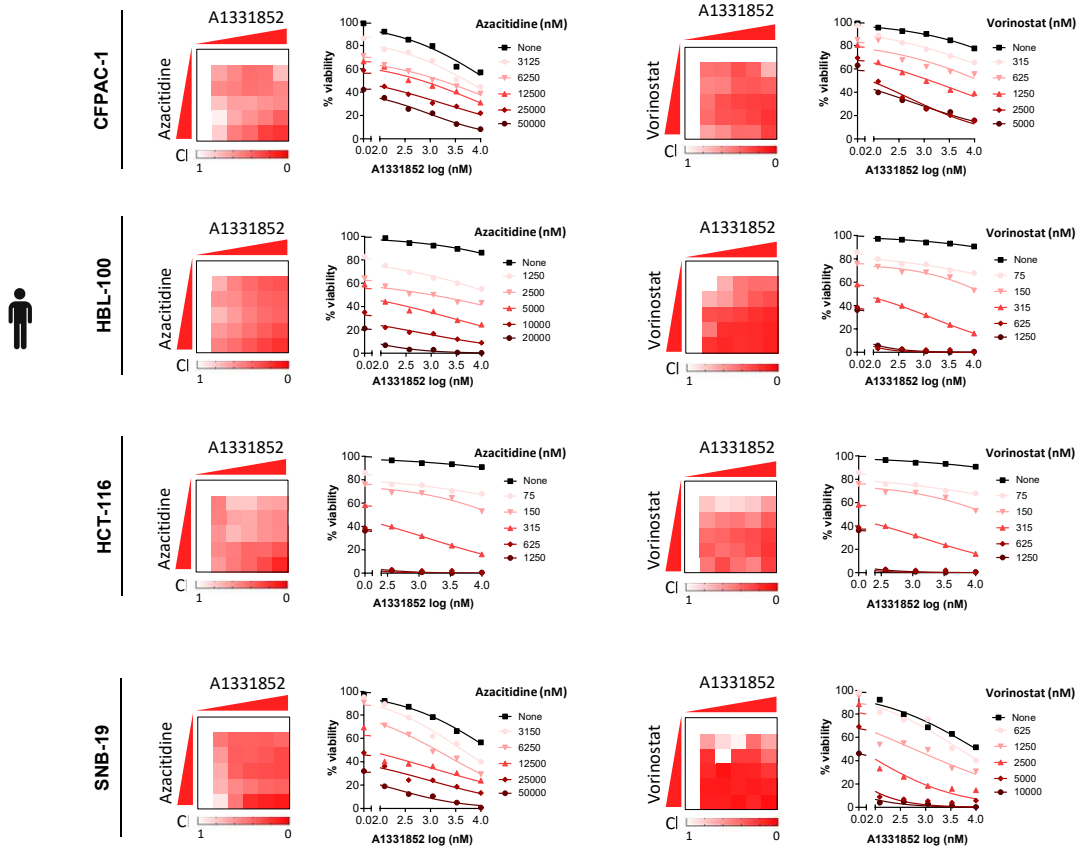

Supplementary Figure 16. Combination index (CI) values and cell viability curves of epigenetic drugs azacitidine (left) or vorinostat (right) with anti-BCL-XL (A1331852) at increasing concentrations in human cancer cell lines of different origins. A synergistic effect between the two drugs was considered when at least four drug-drug interactions had CI values < 1.

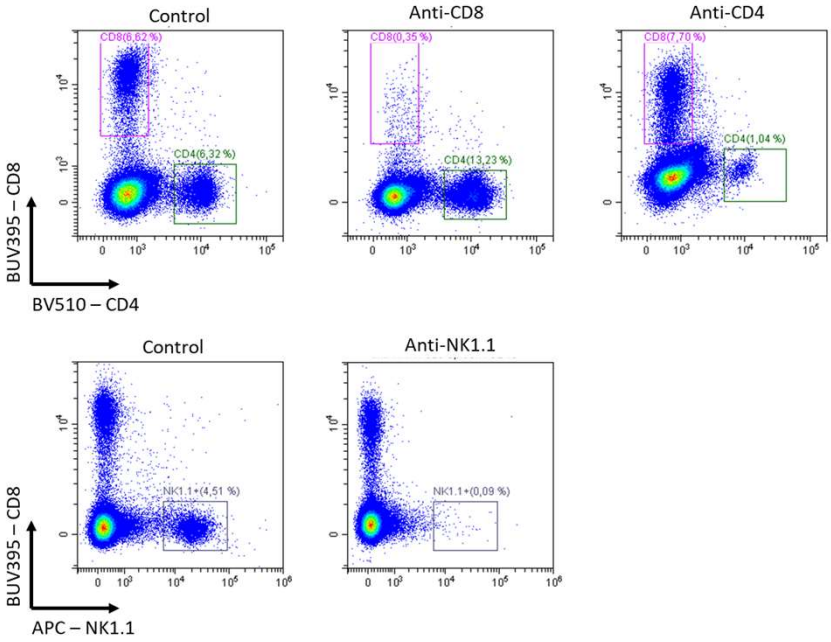

Supplementary Figure 17. Flow cytometry analysis of splenic CD8, CD4 and NK cells from mice treated with the triple combination in the presence or absence of the indicated depleting antibodies. The analysis was performed on day 19 after tumor implantation, at the endpoint of the experiment.

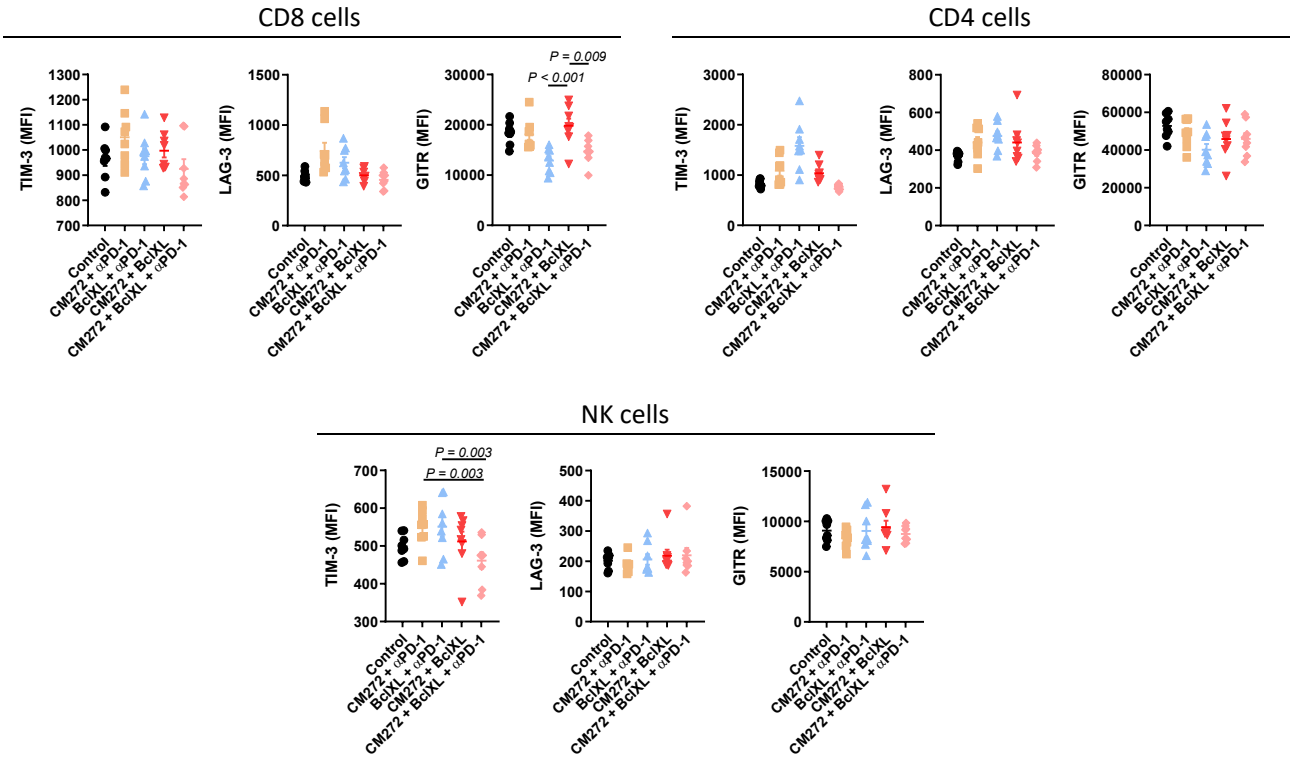

Supplementary Figure 18. Flow cytometry analysis of exhaustion markers in tumor-infiltrating CD8, CD4 and NK cells performed on day 15 after implantation of LLC cells in mice treated with vehicle (control), CM272 (5 days per week, starting on day 5), anti-PD-1 (days 7, 10, 14) and/or A1331852 (3 days per week starting on day 5). Eight mice were used in each experimental group. Data are expressed as mean ± SEM. Comparisons were performed by one-way ANOVA followed by Tukey's post hoc test.

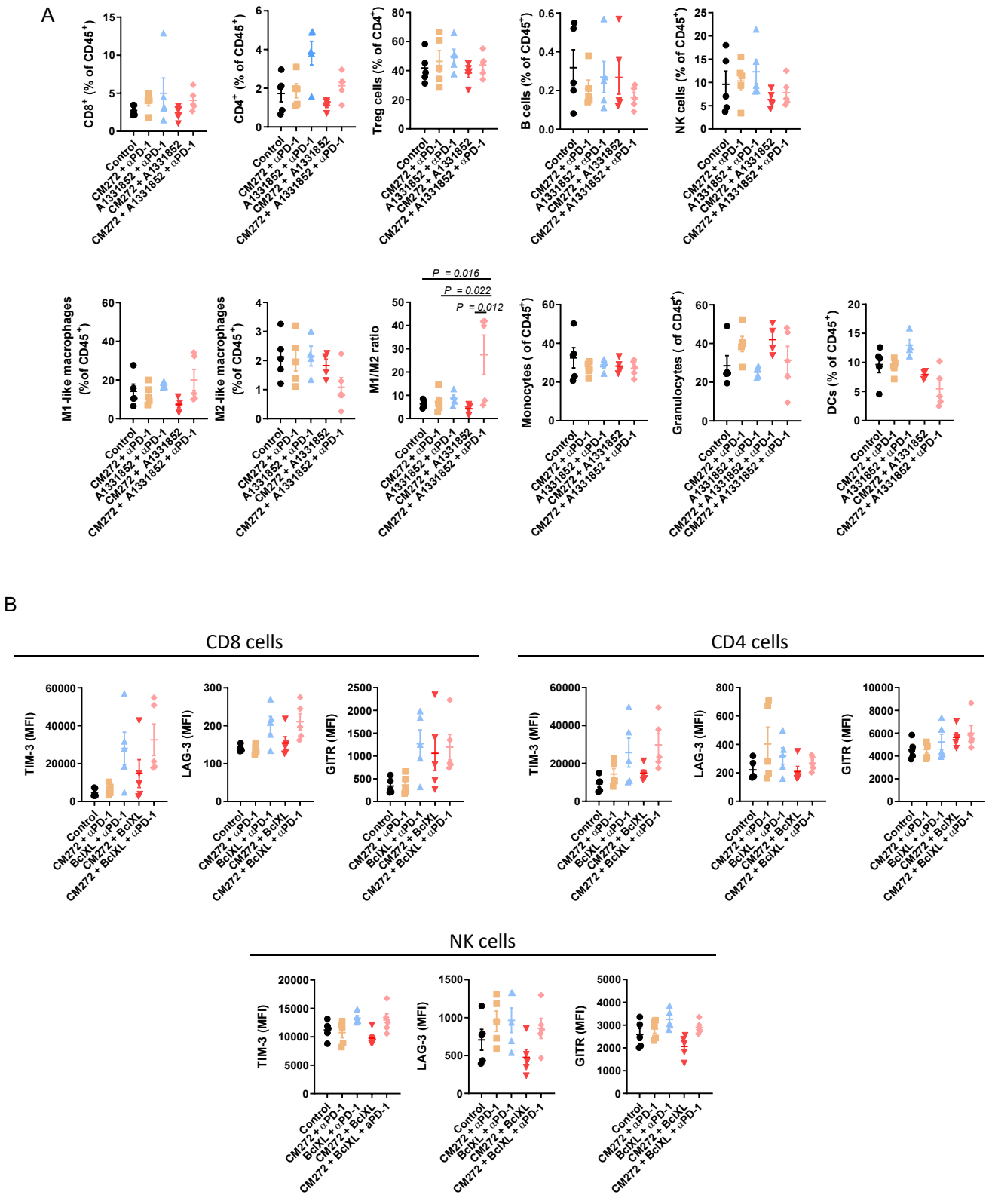

Supplementary Figure 19. A. Flow cytometry analysis of tumor-infiltrating immune cells performed on day 14 after implantation of 393P cells in mice treated with vehicle (control), CM272 (5 days per week, starting on day 5), anti-PD-1 (days 7, 10, 13) and/or A1331852 (3 days per week starting on day 5). Eight mice were used in each experimental group. **B.** Flow cytometry analysis of exhaustion markers in the tumor-infiltrating CD8, CD4 and NK cells. Data are expressed as mean ± SEM. Comparisons were performed by one-way ANOVA followed by Tukey's post hoc test.

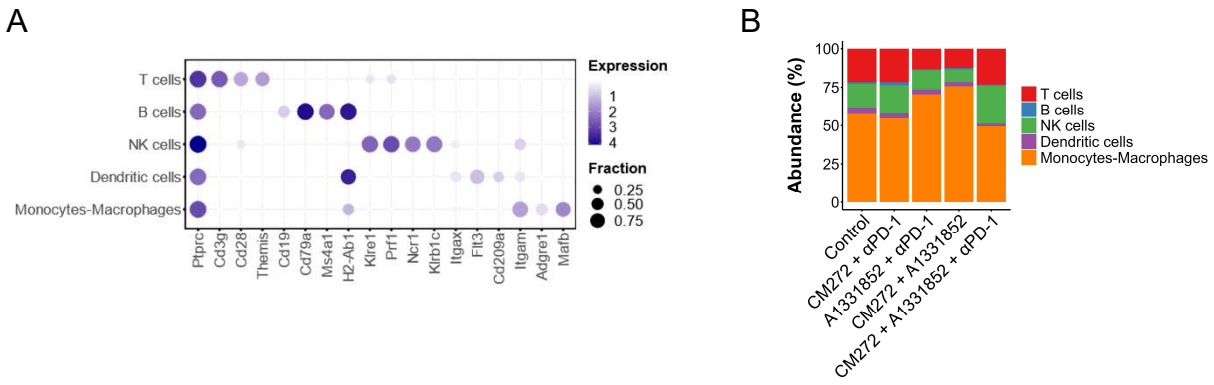

Supplementary Figure 20. A. Dot plot of expression levels of cell-type marker genes in each cell cluster. **B.** Percentage of each cell type observed in the different treatments.

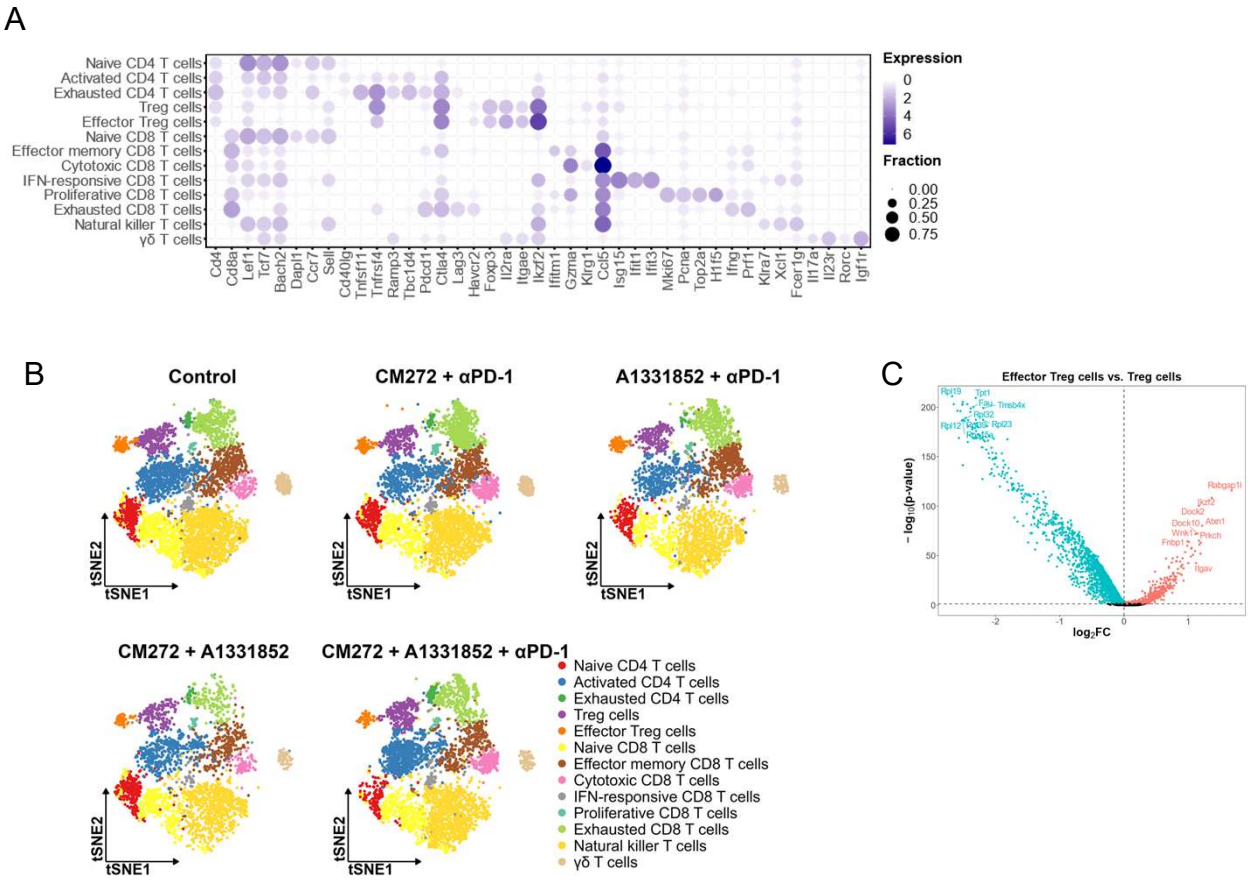

Supplementary Figure 21. A. Dot plot of T-cell marker genes. **B.** Two-dimensional t-distributed stochastic neighbor embedding (t-SNE) plots showing the 13 identified clusters of T cells in the different treatments. **C.** Volcano plot of differentially expressed genes between the two subtypes of Treg cells.

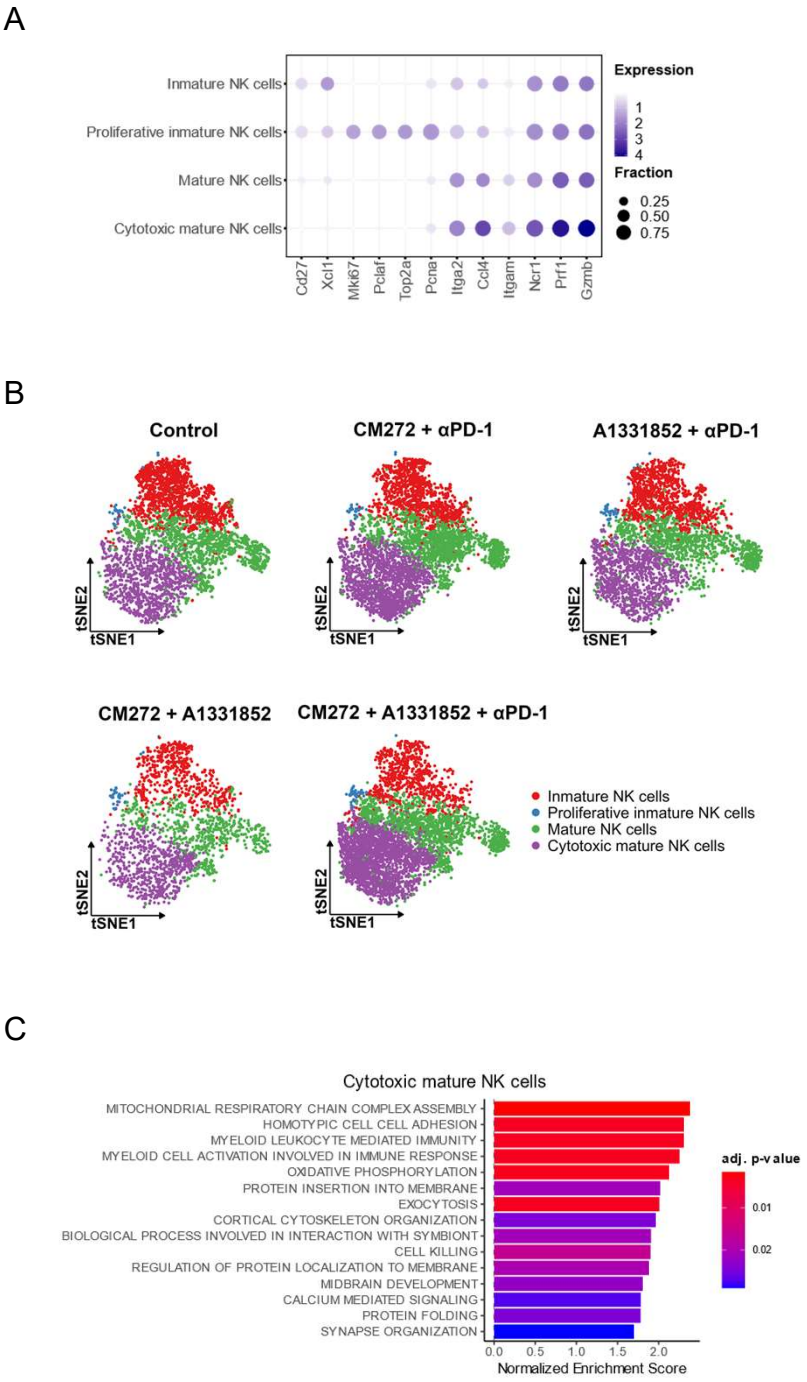

Supplementary Figure 22. A. Dot plot of NK-cell marker genes. **B.** Two-dimensional t-distributed stochastic neighbor embedding (t-SNE) plots showing the four subclusters of NK cells in the different treatments. **C.** GSEA analysis of GO enriched scores in cytotoxic mature NK cells.

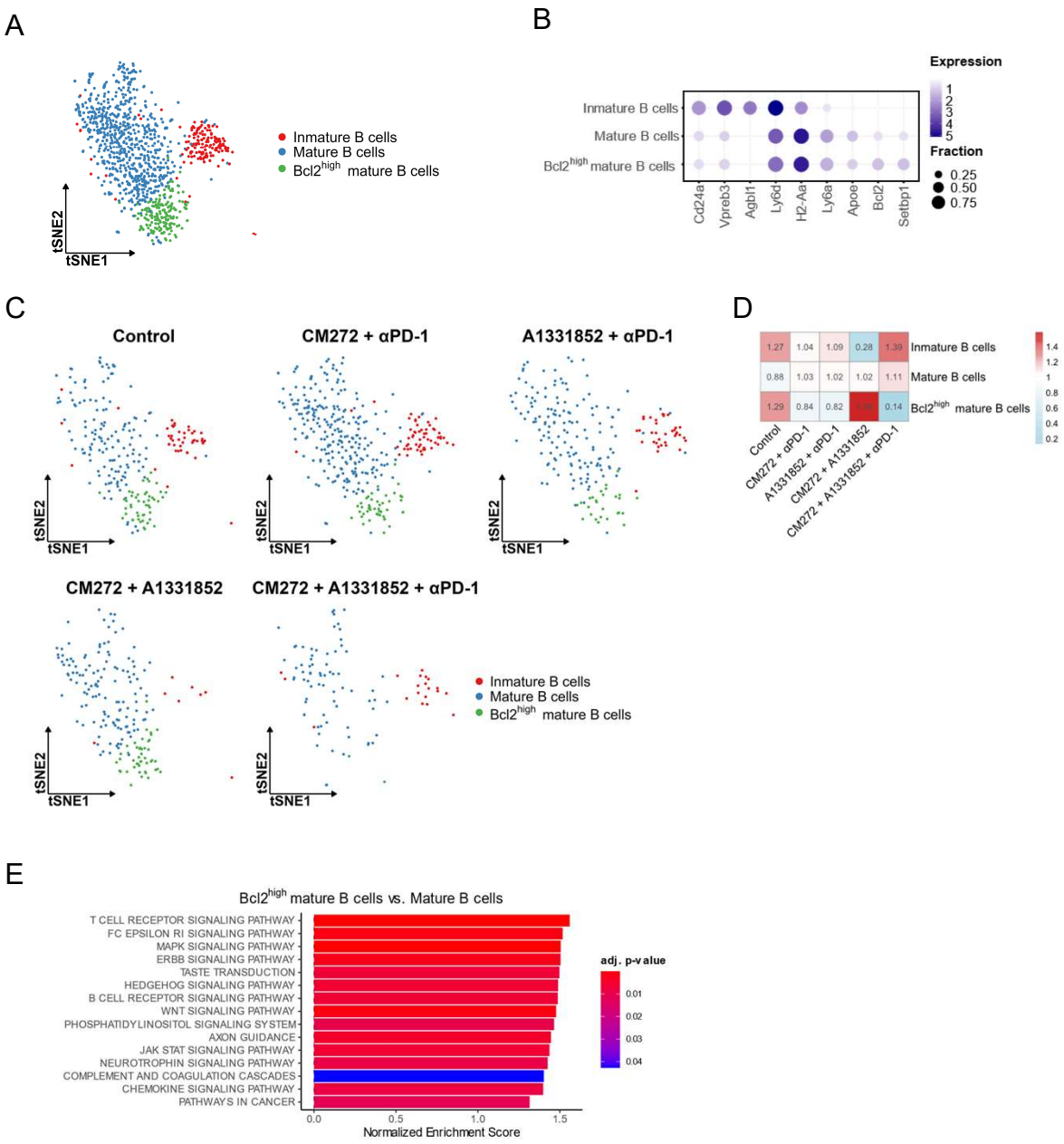

Supplementary Figure 23. A. Two-dimensional t-distributed stochastic neighbor embedding (t-SNE) plot showing the B cell clusters of immune cells in the TME of LLC tumors. **B.** Dot plot of B-cell marker genes. **C.** t-SNE plots showing the three subclusters of B cells in the different treatments. **D.** Prevalence of each B-cell subtype estimated by Ro/e score. **E.** GSEA analysis of enriched KEGG scores in Bcl2^{high} mature B cells.

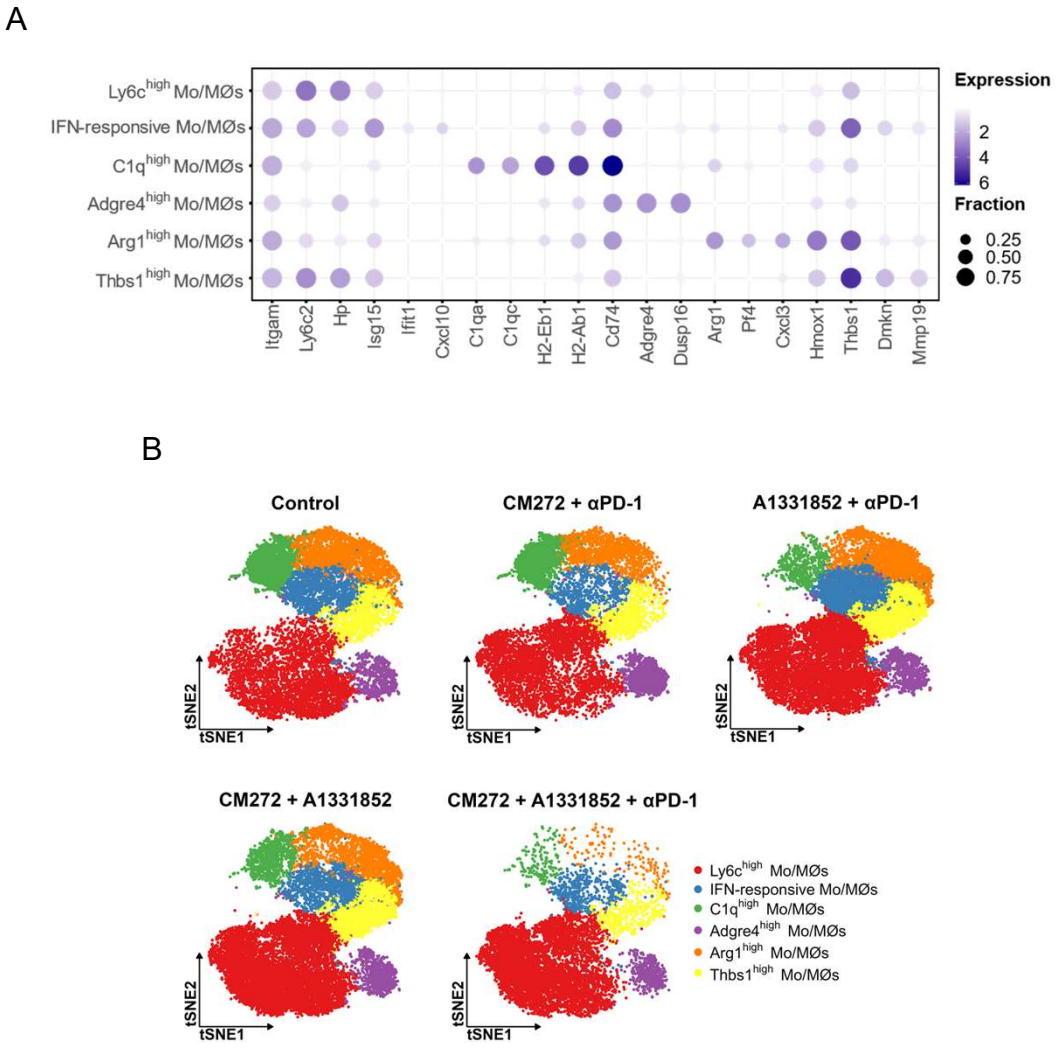

Supplementary Figure 24. A. Dot plot of monocyte/macrophage (Mo/MØ) marker genes. **B.** Two-dimensional t-distributed stochastic neighbor embedding (t-SNE) plots showing the six subclusters of Mo/MØs in the different treatments.

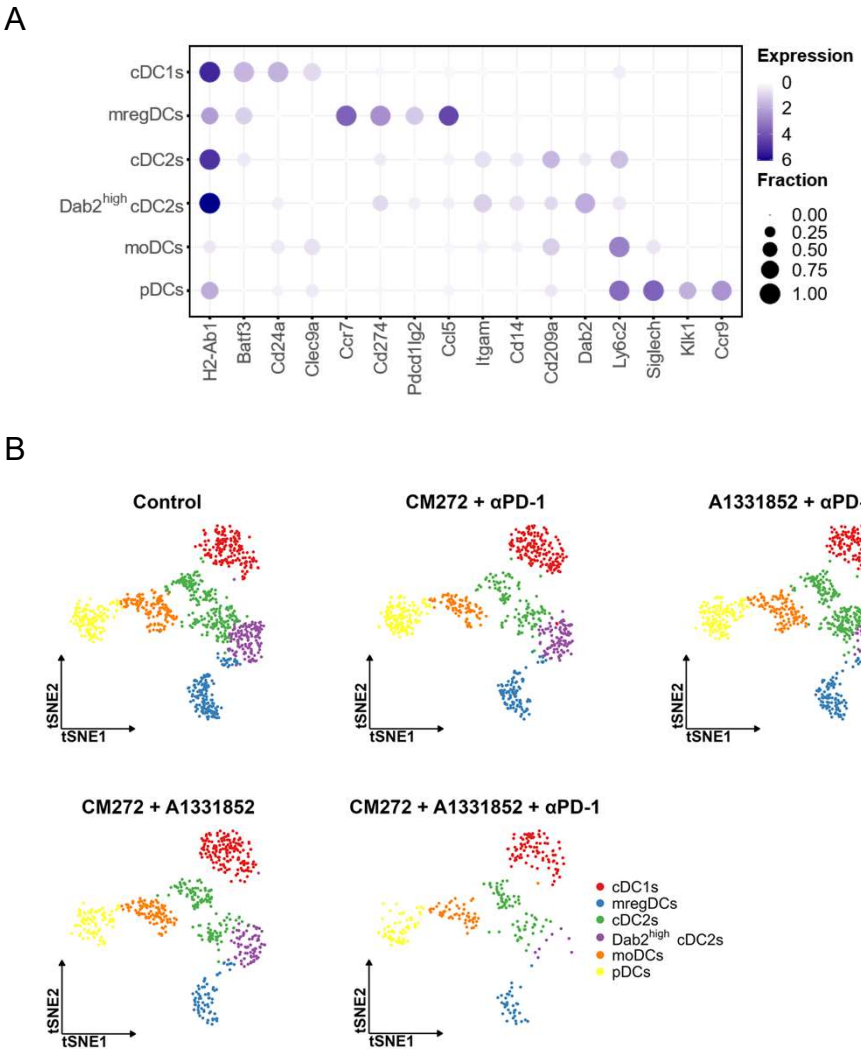

Supplementary Figure 25. A. Dot plot of DC marker genes. **B.** Two-dimensional t-distributed stochastic neighbor embedding (t-SNE) plots showing the six subclusters of DCs in the different treatments.